Asociación Argentina
de Mecánica Computacional

Mecánica Computacional Vol XL, págs. 471-480 (artículo completo)
F.A. Avid, L.C. Bessone, P. Gamazo, J.J. Penco, M.A. Pucheta, M.A. Storti (Eds.)
Concordia, 6-9 Noviembre 2023

CHARACTERIZATION OF FLOW AND DESIGN PARAMETER ANALYSIS USING COMPUTATIONAL FLUID DYNAMICS FOR THE CONSTRUCTION OF A SUBSONIC WIND TUNNEL

Mariovane S. Donini[a], Cristiano H. Schuster[a] and Jean J. Schuster[a]

[a]*Unidad Tecnológica de Automatismos y Sistemas Inteligentes, UTEC ITRN, Rivera, Uruguay, consultas@utec.edu.uy, https://utec.edu.uy/es/*

Keywords: Subsonic Wind Tunnel, Turbulence, Boundary Layer Analysis

Abstract. This work presents a flow characterization for the design guidance of an open-circuit subsonic wind tunnel with a measured working cross-sectional area of 600 mm x 600 mm at the Universidad Tecnologica del Uruguay. The turbulence intensity in the test section and vorticity in the diffuser are analysed using Computational Fluid Dynamics with a $k-\omega\ SST$ turbulence models. It is presumed that the analysis will provide relevant information to improve the wind tunnel design, with emphasis on optimizing the design process of the different sections of this equipment to be constructed by the institution. The expected results include a better understanding of flow patterns and identification of critical points that require adjustments to achieve low turbulence intensity and vorticity, as well as providing fundamental information about the cone and diffuser geometry, as the apparatus is intended to be built. Additionally, the study is expected to contribute to the validation of flow in wind tunnels, providing a solid foundation for future aerodynamic studies on this equipment.

1 INTRODUCTION

In the field of fluid dynamics, a wind tunnel is one of the most valuable tools, because it allows to break the barriers of real word testing and computational fluid dynamics (CFD) simulation.

The Universidad Tecnologica del Uruguay (UTEC) is a relatively new institution, which is creating its plan and lines of development and research, in the fields of control and automation, electric mobility, robotics, energy efficiency, green energy generation and others. All those fields can have a strong component of development and research in aerodynamics, for this reason, the mechanical engineer group of the Control and Automation Engineering chooses to work in this field and considers that having a wind tunnel can collaborate in future work of the university.

The theory of designing a wind tunnel is a subject that has already been extensively explored and developed, and there are many commercial solutions for development and research propose, but the most of them are expensive and not necessarily versatile or customizable for specific applications.

Wind tunnels with a test cross-section greater than 30 cm are not commercially common, even in companies dedicated to research equipment, and usually depend on an on-demand project reflecting on a high cost, so none of the commercial options completely meet the team needs, both in terms of technical characteristics and in economic viability, what leads the team to the decision of designing a completely personalized wind tunnel with cros section of 600 mm x 600 mm. So, the main objective of this work is to characterize the flow of a open-circuit subsonic wind tunnel with 600 mm x 600 mm cross-sectional area, using RANS simulation whit $k-\omega\ SST$ turbulence model to evaluate parameters such as velocity profiles, pressure distributions, turbulence levels, and boundary layer behavior as the first interaction on the design process.

The following sections present a General Specification of Design, where contraction cone and diffuser will be discussed. In the third section Numerical Methods will be covered, where turbulence model, mesh evaluation, solution methods and computational parameters topics will be argued. The fourth section brings the Results discussion, starting with the flow characterization, followed by the stability in the diffuser, closing with turbulence intensity and boundary layer thickness. To close the work, in the fifth section the conclusion will be presented.

2 GENERAL SPECIFICATIONS OF DESIGN SECTIONS

2.1 Contraction Cone

The inlet contraction plays a pivotal role in influencing the flow quality within the test section. It serves to help and align the flow entering the test section. The dimensions and configuration of the contraction exert control over the ultimate turbulence intensity levels within the test section, as emphasized by Derbunovich et al. (1987).

Bell and Mehta (1988) discussed the optimum wall shape for a contraction cone. The contraction wall shape satisfying most of the requirements analysed is clearly the one given by the 5th order polynomial as Eq. (1).

$$Y(X) = H_i - (H_i - H_e)[6(X')^5 - 15(X')^4 + 10(X')^3] \tag{1}$$

where H_i is the contraction height at inlet, H_e is the contraction height at exit and X' is the non-dimension streamwise distance, X/L, where L is the contraction length. The amount

of flow acceleration and reduction of non-uniformities predominantly hinge on the contraction ratio, denoted as N, which quantifies the ratio between the entrance and exit section areas (Ahmed, 2013). In this study, the parameters were chosen to yield a ratio of $N = 2.66$. Initially, the contraction length was set at $1m$ in accordance with the space constraints of the wind tunnel within the university laboratory.

2.2 Diffuser

The primary purpose of diffusers is to restore static pressure, thereby enhancing the efficiency of the wind tunnel and facilitating the closure of the circuit. It is imperative to ensure continuous flow attachment to optimize pressure recovery efficiency. In the event of flow detachment, pressure pulsations propagate upstream into the test chamber, leading to non-uniformities in pressure and velocity.

Considering the aforementioned factors and given the ratio L/H_i (where H_i is determined by the test section size), the corresponding value of aspect ratio (AR) is chosen from the no-stall regions (Cattafesta et al., 2010). In the context of this article, the relationship between the area ratio (AR) at the exit and entrance of the diffuser is examined in correlation with the ratio of diffuser length to the entrance height (LD/H_i). Runstadler et al. (1975) presents this relationship and reveals three distinct regions of design. The no appreciate stall region, unsteady flow and stall region.

When designing the diffuser, it is essential to choose an appropriate length for it, taking into account the constraints imposed by the facility's size limitations. Specifically, the diffuser's length is determined within the confines of the facility's dimensions. Once the (LD/H_i) ratio is established, which is constrained by the height of the test section, the corresponding AR value is selected from the regions where stall is not encountered.

While it is possible to achieve higher pressure recovery by operating in the "unsteady flow" regime, this approach can introduce unwanted noise and result in suboptimal performance under off-design flow conditions. The design point for the diffuser analysed in this study is found to lie on the "no appreciable stall" region, with $L/H_i = 6$ and $AR = 1,77$.

3 NUMERICAL METHOD

The commercial ANSYS Fluent numerical code was employed to predict the flow characteristics within the open-loop subsonic wind tunnel. Figure 1 illustrates the numerical domain along with the specification of each boundary condition and wind tunnel section. A uniform boundary condition of the calculated velocity at the intake of the contraction cone was applied along the inlet surface (velocity inlet), while the outlet (pressure outlet) was set to zero gauge pressure. The no-slip condition was applied at the walls, showed as red lines in Figure 1.

A detailed investigation of peripheral components in the wind tunnel, including honeycomb flow conditioning, exhaust fan, and noise suppressor, was not within the scope of this study.

3.1 Turbulence modelling

The Navier-Stokes (N-S) equations that describe the fluid flow surfer from a closure problem, that means the number of unknown parameters are greater than the number of equations, imposibiliting the solutions of the system. Therefore, two options are available: approximate the solution evaluating all the scales of turbulence through a Direct Numerical Simulation (DNS), that is time and computational-cost prohibitive; or use a closure method through modelling the turbulence scales.

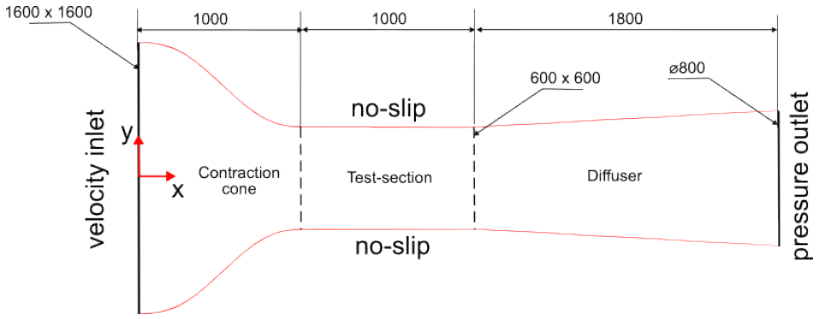

Figure 1: Numerical domain. All dimensions in $[mm]$.

In this work the flow is approximated by a Reynolds-Averaged Navier-Stokes (RANS) equations, while a two equation turbulence model is used to represent the effects of the turbulence: one for the transport of the turbulent kinetic energy (k); an another for transport variables depending of the type of the model used, more often turbulent dissipation. Between the options available, a $k-\omega$ Shear Stress Transport ($k-\omega\ SST$) was elected.

For the $k-\omega\ SST$ model, one of the two equations mentioned early, is used to model the transport of k, as can be seen in the Eq. 2. All the governing equations will not be reiterated here, but can be found in ANSYS (2009).

$$\frac{\partial}{\partial t}(\rho k) + \frac{\partial}{\partial x_i}(\rho k u_i) = \frac{\partial}{\partial x_j}\left(\Gamma_k \frac{\partial k}{\partial x_j}\right) + G_k - Y_k + S_k + G_b \tag{2}$$

While the dissipation of turbulence (ω) will be modeled by the Eq. 3.

$$\frac{\partial}{\partial t}(\rho \omega) + \frac{\partial}{\partial x_i}(\rho \omega u_i) = \frac{\partial}{\partial x_j}\left(\Gamma_\omega \frac{\partial \omega}{\partial x_j}\right) + G_\omega - Y_\omega + D_\omega + S_\omega + G_{\omega b} \tag{3}$$

Both Eq. 2 and 3 will be used near the wall, wile in the free stream a $k-\epsilon$ will be used, as explained further in this section. The G in the above equations stands for k and ω generation, while Y represent the dissipation of both quantities, the S accounts for source terms while G_b and $G_{\omega b}$ represents the effects of buoyancy, whereas D_ω accounts the cross-diffusion term in the turbulence dissipation (Eq. 3).

The choice for the $k-\omega\ SST$ was made because it blends the best of the $k-\epsilon$ and $k-\omega$ models, once it do not need a wall damping function that is needed in the $k-\epsilon$ model, that proven to be unreliable in a variety of flows, especially when large pressure gradients are present, and it overcome the high dependence of the solution values sensitiveness of the free-stream values of the turbulence applied to the inlet of the domain present in the $k-\omega$ model. For both, $k-\epsilon$ and $k-\omega$ models, it is well known that the separation over smooth surfaces of bodies is not accurate when compared with experimental data, mainly because the shear stress computed is too high (Menter, 1992).

So, the $k-\omega\ SST$ is a blend by $k-\omega$ model, were the last one is used near the walls, and the $k-\epsilon$, that actuates in the free stream of the flow. This is achieved by using blending functions, F_1 and F_2 in this case, similar to first proposed by Menter (1993). Those blending functions are a hyperbolic tangent function, for F_1, the hyperbolic tangent argument is close related by the distance of the walls, when this function result in one, the $k-\omega$ will bi used, whereas the result is zero, the $k-\epsilon$ is used, anything in between will be blended.

$$\begin{aligned} F_1 &= tanh(\Phi_1^4) \\ F_2 &= tanh(\Phi_2^2) \end{aligned} \tag{4}$$

The second blending function, F_2, is similar to F_1, and have the function to limit the turbulent viscosity, Eq.5, of the model.

$$\mu_t = \frac{\rho k}{\omega} \frac{1}{max\left[\frac{1}{\alpha}, \frac{SF_2}{a_1 \omega}\right]} \tag{5}$$

Where the F_2 is the blending function and S is the strain rate magnitude. If F_2 or S is large, the turbulent viscosity μ_t is reduced.

3.2 Computational mesh

The work integrated the benefits of a structured mesh with sizing refinement in the wind tunnel's wall direction to reduce computational expenses. While both 2D and 3D cases were considered, the absence of stall conditions in the 3D cases led to a predominant use of the 2D geometry for other calculations, given the plane symmetry nature of the flow. This approach was adopted to avoid incurring unnecessary computational costs.

With the motivation of ensuring the description of wall effects in the flow at the test section along with the turbulence modelling discussed above, the mesh independency test was realized around the dimensionless wall distance parameter y^+. One can interpret y^+ as a local Reynolds number, indicating that its magnitude is likely to govern the relative significance of viscous and turbulent phenomena (Schlichting and Gersten, 2016). The adimensional wall distance is calculated by $y^+ = yu_\tau/\nu$, where u_τ is the so-called friction velocity, y is the absolute distance from the wall and ν is the kinematic viscosity.

Figure 2a illustrates various cases of y^+ used for analysing the impact of mesh refinement on the description of the boundary condition. Both the x and y axes of Figure 2a employ a logarithmic scale to accentuate the distinctions between the curves. The selected mesh for this study is depicted by the red diamond curve, and it is detailed in Figure 2b.

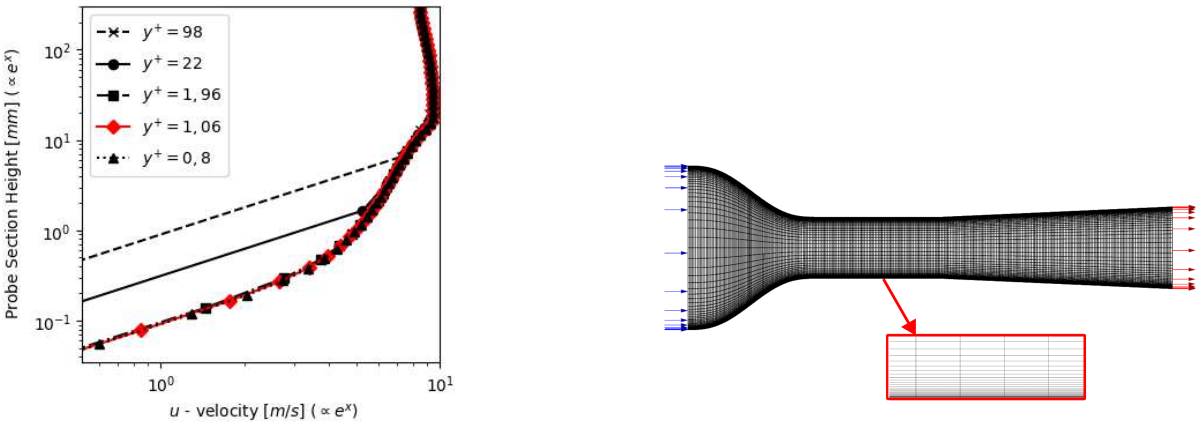

(a) Mesh refinement analysis.

(b) Detailed mesh and flow direction.

Figure 2: Computational mesh.

3.3 Solution methods

In this work a Finite Volume Method (FVM) will be used through ANSYS® Fluent® 2022 R2. The spatial discretization will be done by values of scalar stored in cell center, however, cell

face values must be interpolated from cell center for convective terms in scalar transport equations, like for k, ω and space decomposed momentum, done by the QUICK scheme described in the following.

To solve the pressure and velocity along the domain, a Semi-Implicit Method for Pressure Linked Equations Consistent (SIMPLEC) will be used to discretize the partial differential governing equations, like conservation of mass and momentum, in algebraic coupled equations, so it will be possible to solve numerically in a finite volume discrete mesh. The pressure and velocity equations are coupled through pressure terms in the components of the momentum equations, and the pressure is treated implicitly, meaning that solutions for pressure and velocity are found iteratively (Shen et al., 2003).

A Least Squares Cell Based method was used for the calculation of the gradients and derivatives, where in this method the solution is assumed to vary linearly based on the centroid cell evaluation. While the pressure was discretized by Second-Order method to avoid discretization error for eventual misalignment between flow and mesh, and to get better results in general. For momentum, k and ω, the QUICK method was chosen because it is appropriate for hexahedral meshes, in case no hexahedral cells will be found, a Second-Order Upwind discretization will be applied into those cells automatically (He et al., 2014).

3.4 Computational parameters

In order to control the convergence rate and stability of the solution, some parameters known as "under-relaxation factors" (URF) can be used to decelerate the convergence, being often utilized to avoid divergence in the iterative solution of strongly nonlinear equations. These factors are applied to the updated values of flow variables, like velocity and pressure, during each iteration of the numerical solver, aiming to adjust the contribution of the new solution values relative to the previous ones in order to control the convergence behavior of the solver (Patankar, 1980).

When URF is set to 1.0, it means that the new field value is fully accepted in each iteration, while URF is less than 1.0, only a fraction of the new value of the field is used to update the solution. The correct election of the URF can help stabilize the convergence process and prevent oscillations, and is chosen depending on the complexity of the flow, like turbulence intensity, geometry of the domain, among other factors. In this work a relatively simple geometry is used whit a laminar flow, and the URF was set to $0,3$ for the pressure, $0,7$ for momentum, $0,8$ for k and ω equations, while for μ_t equation it was set to 1, and integrally accepted new values in each iteration.

Each cell in the domain was initialized before the simulation whit base in the inlet velocity ($\approx\ 3,28\ m/s$) along the x (streamwise) direction. That velocity resulted a initialization of $k \approx 0.0403\ m^2/s^2$ and $\omega \approx 276\ s^{-1}$ in each cell.

A steady state simulate was used, were one thousand iteration were conducted. The convergence was ensured by the values of all equations (continuity; x, y and z velocity; k and ω) absolute residuals being below 10^{-5}.

4 RESULTS

4.1 Flow Characterisation

Flow characterization in a wind tunnel is a critical aspect of experimental aerodynamics. It involves a comprehensive assessment of the airflow properties within the tunnel, encompassing parameters such as velocity profiles, pressure distributions, turbulence levels, and boundary

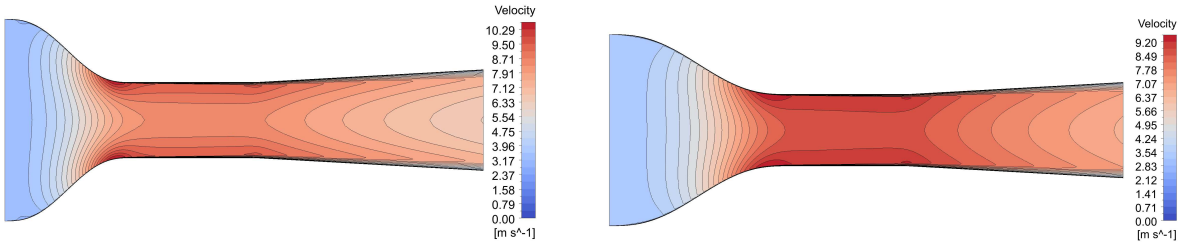

(a) Contraction cone A: $L_{cone} = 1m$ (b) Contraction Cone B: $L_{cone} = 1,5m$

Figure 3: Velocity magnitude.

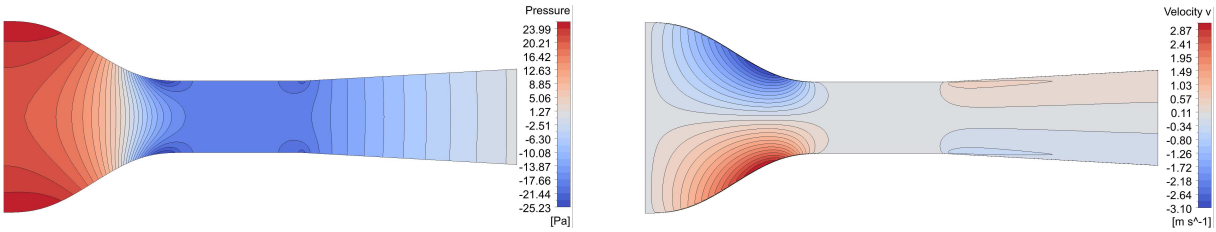

(a) Static Pressure (b) V - Velocity

Figure 4: Flow characterizing variables.

layer behaviour. Figure 3 shows the contour plot for velocity magnitude in two wind tunnel contraction cones design. The design A has a length of $1m$ and B, $1,5m$. All subsequent findings pertain to contraction cone B, given its milder flow conditioning and reduced impact of non-uniform flow at the test section exit.

The drive system selected for this wind tunnel is an industrial air extractor fan of $800mm$ of diameter with 1450 rpm. Fans are evaluated based on their capacity to handle volume flow rates and static pressure drops. Figure 4a shows the static pressure contours in $[Pa]$ for Case 4, which represents the most demanding scenario for the drive system. This case necessitates the maximum flow rate to attain the desired test-section velocity. In this case, the pressure loss is approximately $24Pa$.

Static pressure loss analysis, as described by Barlow et al. (1999), forms the basis for the wind tunnel performance curve, delineating pressure loss at varying flow rates. Operational states are established at convergence points, emphasizing the importance of aligning them with the fan's peak efficiency for optimal performance.

Besides the pressure loss, the contours of static pressure (Fig. 4a indicates a region with absence of gradients in the test section. This region serves to minimize unwanted variations in pressure, thereby allowing researchers to isolate and study the specific effects of the aerodynamic features under investigation. To highlight the presence of a uniform velocity region within the test section, Figure 4b illustrates the vertical velocity component. By extracting the area devoid of vertical velocity within the test section via contour plotting, it is revealed that the effective test section length is approximately 15% shorter than the originally projected length. This underscores the importance of accurately identifying and characterizing the region with uniform flow conditions for precise experimentation and measurements.

4.2 Diffuser Stability

As mentioned in the Section 2, the test section is greatly influenced by the design of the diffuser. The absence of vortices at the diffuser is illustrated by Figure 5 which displays the dimensional vorticity z-component defined by

$$\omega = \frac{\partial v}{\partial x} - \frac{\partial u}{\partial y} \tag{6}$$

Large negative regions detached from the wind tunnel wall could indicate clockwise vortex structures, while positive regions may denote counterclockwise vortex structures. However, this phenomenon does not occur in this diffuser design, as illustrated in Figure 5, and in accordance with Section 2.2. This is attributed to the fact that vorticity change only takes place at the walls under the influence within the boundary layer, characterizing the no-stall regime.

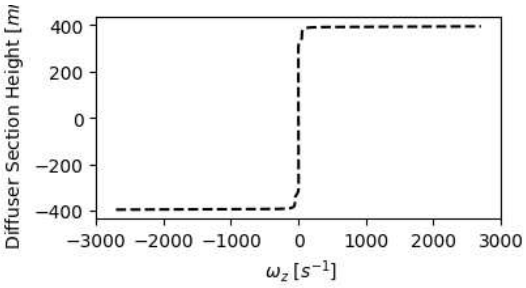

Figure 5: Dimensional vorticity.

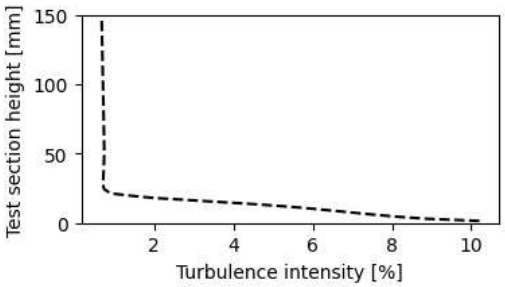

Figure 6: Turbulence intensity at $L = 2m$.

4.3 Turbulent Intensity

Discrepancies observed in test results conducted at identical Reynolds numbers in different wind tunnels and between wind tunnel tests, and in-flight experiments have suggested the necessity for corrections to account for the turbulence present in wind tunnels. It has been proposed that this turbulence induces flow patterns in the tunnel, akin to those found in free air at a higher Reynolds number. Consequently, the Reynolds number used in tunnel tests could be regarded as an elevated "effective Reynolds number" (Barlow et al., 1999).

In numerous facilities, by the above, maintaining low turbulence levels within the test section is of paramount importance. Wind tunnel experiments frequently aim to isolate the impacts of incoming freestream turbulence, a goal shared by various applications in the current project.

The turbulence intensity, also often referred to as turbulence level, is defined as $I \equiv \frac{u'}{U}$ where u' is the root-mean-square of the turbulent velocity fluctuations and U is the mean velocity (Reynolds averaged). If the turbulent energy, k, is known, u' can be computed as

$$u' \equiv \sqrt{\frac{1}{3}\left(u_x'^2 + u_y'^2 + u_z'^2\right)} = \sqrt{\frac{2}{3}k} \tag{7}$$

Results indicate a turbulence intensity of approximately 10% at the boundary condition, highlighting a substantial level of turbulence, as shown in Figure 6. In contrast, the symmetry line exhibits a significantly lower turbulence intensity of approximately $0,71\%$. Higher turbulence intensity levels (above 5%) are generally less desirable, as they can introduce more uncertainty and variability in the test results (Ahmed, 2013).

The low turbulence intensity along the symmetry line suggests an area of relative stability. This finding is consistent with theoretical expectations, confirming the efficacy of the wind tunnel design in maintaining a controlled flow environment.

4.4 Boundary Layer Thickness

Another critical aspect in wind tunnel design is the boundary layer thickness. This parameter was investigated using CFD simulations, employing the recorded boundary conditions. Subsequently, a comparison was conducted with the analytically calculated values.

As per Barlow et al. (1999), it can be reasonably assumed that all tunnel boundary layers are predominantly turbulent. Instances where the transition locations on surfaces are specifically sought after are exceedingly rare. Hence, all calculations pertaining to the boundary layer in the flow section were conducted under the assumption of a turbulent boundary layer. Based on the Blasius solution, the boundary layer thickness at the specified location in the flow section can be analytically determined using the following equation $\delta = 0.38x/Re_x^{1/5}$.

Figure 7 illustrates a comparison between the boundary layer thickness derived from the Blasius solution (represented by lines), and the results obtained through CFD simulation (represented by symbols), presented in terms of flow section length. A high degree of qualitative correlation was observed between the two datasets. The primary disparity between the analytical and CFD findings arises from the non-uniform incoming velocity at the test section entrance in the latter case. The disparities in values arise because the Blasius solution assumes a Boundary Layer on a Flat Plate, which may not fully capture the complexities of the actual flow conditions.

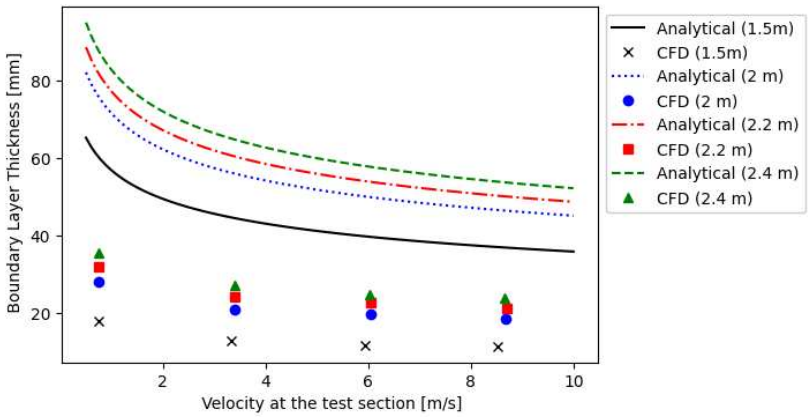

Figure 7: Boundary Layer Thickness at different cross-sections at the test section.

Furthermore, a distinct feature is discernible in the form of a third structure within the boundary layer, as illustrated in Figure 2a. This additional structure is attributed to the influence of the unbounded boundary layer, originating from the accelerated flow that diverts upon exiting the contraction cone. Hence, the description outlined herein defines the inertial region within the boundary layer. The two structures beneath the peak velocity in Figure 2a represent the viscous domain, comprehending the viscous sublayer and buffer layer denoted here as the first structure, as well as the logarithmic layer identified as the second structure. The phenomenon that produce this third structure introduces an additional layer of complexity to the flow behaviour within the boundary layer. Further investigation is warranted to better understand and quantify this effect of inertial regions.

5 CONCLUSIONS

The initial CFD analyses streamlined the design process, enabling a holistic evaluation of the wind tunnel from the contraction cone to the diffuser. This approach contrasts with the need for segmented sections and less precise control conditions in analytical analyses. By examining this complete system, we gained valuable insights into boundary layer development across different sections, particularly its impact on the area of interest.

The study elucidated the influence of contraction cone length on velocity profiles. A 1.5m cone demonstrated less variation in velocity within the test section, making it the preferable choice.

Our investigation has revealed that aspects such as boundary layer thickness, velocity uniformity, and turbulence levels significantly influence the quality and reliability of wind tunnel experiments. It is evident that the design and configuration of critical components, including the contraction cone, play a crucial role in shaping the flow characteristics within the test section. Acknowledging the nuances and deviations from theoretical models, as observed through CFD simulations, underscores the need for continual refinement and optimization of wind tunnel setups to ensure accurate and consistent results. Overall, this study highlights the intricate interplay of factors that govern the behaviour of aerodynamic flows within wind tunnels, providing valuable insights for both research and practical applications in the field of aerospace engineering.

REFERENCES

Ahmed N. *Wind tunnel designs and their diverse engineering applications*. BoD–Books on Demand, 2013.

ANSYS. *ANSYS FLUENT Theory Guide*. ANSYS, Inc., release 12.0 edition, 2009. Available at https://usermanual.wiki/Document/ANSYSTheoryGuide.39891911.pdf.

Barlow J.B., Rae W.H., and Pope A. *Low-speed wind tunnel testing*. John wiley & sons, 1999.

Bell J.H. and Mehta R.D. Contraction design for small low-speed wind tunnels. Technical Report, 1988.

Cattafesta L., Bahr C., and Mathew J. Fundamentals of wind-tunnel design. *Encyclopedia of aerospace engineering*, pages 1–10, 2010.

Derbunovich G., Zemskaya A., Repik E., and Sosedko Y.P. Effect of flow contraction on the level of turbulence. *Fluid Dynamics*, 22(2):289–294, 1987.

He S.H., Liu D.Y., and Tan D.L. Comparison of various spatial discretization schemes in numerical simulation for ship airwakes. *Applied Mechanics and Materials*, 627:63–68, 2014.

Menter F. Zonal two equation kw turbulence models for aerodynamic flows. In *23rd fluid dynamics, plasmadynamics, and lasers conference*, page 2906. 1993.

Menter F.R. Improved two-equation k-omega turbulence models for aerodynamic flows. Technical Report, 1992.

Patankar S.V. *Numerical heat transfer and fluid flow*. Hemisphere Publishing Corporation, 1980.

Runstadler P.W., Dean R.C., and Dolan F.X. *Diffuser Data Book: Diffuser Data and Interpretation*. Creare, Incorporated, 1975.

Schlichting H. and Gersten K. *Boundary-layer theory*. springer, 2016.

Shen W.Z., Michelsen J.A., Sørensen N.N., and Nørkær Sørensen J. An improved simplec method on collocated grids for steady and unsteady flow computations. *Numerical Heat Transfer: Part B: Fundamentals*, 43(3):221–239, 2003.